Electrocatalysis (2019) 10:134–148
https://doi.org/10.1007/s12678-018-0503-1

ORIGINAL RESEARCH

Non-Noble Fe-N_x/C Electrocatalysts on Tungsten Carbides/N-Doped Carbons for the Oxygen Reduction Reaction

Ulisses A. do Rêgo [1,2] · Thiago Lopes [3] · José L. Bott-Neto [1] · Ana M. Gómez-Marin [1] · Auro A. Tanaka [2] · Edson A. Ticianelli [1]

Published online: 1 December 2018

Abstract

This work investigates the influence of different nitration protocols of a carbon black, the addition of tungsten carbide (WC), and the presence of iron, in terms of the catalytic activity of electrocatalysts containing Fe-N_x moieties towards the oxygen reduction reaction (ORR) in acidic and alkaline media. The synthesized materials were characterized using X-ray diffraction (XRD), Raman spectroscopy (Raman), energy-dispersive X-ray spectroscopy (EDX), transmission electron microscopy (TEM), X-ray photoelectron spectroscopy (XPS), and cyclic voltammetry (CV) with a rotating ring-disk electrode (RRDE), in addition to durability tests. In acidic media, the performance of the catalysts varied according to the type of nitration protocol, the presence of iron, and the heat treatment temperature, which is accompanied by variations in the ORR mechanism. In alkaline electrolyte, the electrocatalysts presented higher performances, with only an ~0.04-V difference relative to that of a standard platinum on carbon catalyst. The number of electrons transferred per oxygen molecule, the amounts of hydrogen peroxide generated in the ORR, the effect of catalyst loading, and the presence of iron in the catalysts were investigated with the aim of understanding the ORR mechanism and assisting in the production of high-performance and durable materials. Finally, the two best electrocatalysts were submitted to a standard durability test, which evidenced promising high stability at both pHs.

Keywords Non-noble metal catalysts · Fe-N_x catalysts · Oxygen reduction · Acid media · Alkaline media

Introduction

The oxygen reduction reaction (ORR) is an important and complex electrochemical reaction that takes place in fuel cells and in metal/air battery systems, among other devices. For such systems, a most efficient catalyst for the promotion of this reaction consists of Pt nanoparticles supported on a suitable high surface area carbon powder. Different types of carbon blacks, activated carbon, and graphite have been used as supports for noble metal catalysts. These supports present primary roles in defining both the activity and the stability of the catalyst/active site. The surface properties of these supports determine the degree of dispersion of the noble metal nanoparticles, with a heterogeneous carbon surface leading to the greatest surface area.

Several studies have shown that the treatment of carbon supports with nitrogen species, i.e., HNO_3 and NH_3, can dramatically increase the catalytic activity of electrocatalysts towards the ORR [1–5]. This is promoted by the introduction of nitrogenous groups and modification of the carbon with oxygen species, which may also promote the introduction of nitrogen [1–5]. This is given by the basic character of the carbon, associated with the resonance of the π bonds of the aromatic carbon ring [5–7], which may favor the attack of oxygen moieties by free radicals such as NH_2, NH, H, and N that are produced by decomposition of ammonia at high temperatures, which in turn further promotes the formation of nitrogen groups on the carbon surface [5, 8, 9].

Electronic supplementary material The online version of this article (https://doi.org/10.1007/s12678-018-0503-1) contains supplementary material, which is available to authorized users.

✉ Thiago Lopes
tlopeschem@gmail.com

[1] Instituto de Quimica de Sao Carlos, Universidade de Sao Paulo, Sao Paulo, SP 13560-960, Brazil

[2] Universidade Federal do Maranhão, São Luis, MA 65080-040, Brazil

[3] Instituto de Pesquisas Energéticas e Nucleares, IPEN/CNEN-SP, Sao Paulo, SP 05508-000, Brazil

Recent studies have highlighted tungsten carbide as a promising support of noble metal catalysts towards the ORR in acid media [10, 11], since it is stable, cost-effective, and tolerant to poisoning by H_2S and CO poisonings [12–15]. However, in order to reduce the costs associated with the use of noble metals and to develop cheap and active electrocatalysts for the ORR, tungsten carbides have also been tentatively tested in conjunction with promising non-precious metal catalysts, such as Fe [16] and/or Co [17], together with a nitrogen source, in a carbonaceous matrix and produced by pyrolytic treatments at temperatures varying in the range of 600 to 1000 °C [18–22]. Although several studies have been carried out using N-doped carbon electrocatalysts, there have been no studies investigating this treatment applied to tungsten carbide materials for use as non-noble catalysts.

In this work, different non-noble metal hybrid materials formed by tungsten carbide/N-doped carbons and non-noble metal structures (Fe-N_x or NC) were evaluated as electrocatalysts for the ORR. To this end, tungsten carbide/N-doped carbons were prepared by first doping a carbon black powder with nitrogen groups, followed by the impregnation of a tungsten precursor and its carburization. This was followed by incorporation of an iron complex, after which the composite was thermally treated for activation and stabilization of the Fe-N_x species. Various physical techniques such as X-ray diffraction (XRD), Raman spectroscopy (Raman), energy-dispersive X-ray spectroscopy (EDX), transmission electron microscopy (TEM), and X-ray photoelectron spectroscopy (XPS) were employed for the characterization of the catalysts. Electrochemical tests were carried out to determine the catalytic activities of the hybrid electrocatalysts towards the ORR in acid and alkaline electrolytes, in addition to cyclic voltammetry and durability assays.

Experimental Section

Synthesis of the Supports

Tungsten carbide/N-doped carbon supports were synthesized in two steps, as shown in Fig. 1a. In the first step, the N-doped carbon was performed by three different procedures. In the first of these steps, carbon nitriding was performed by means of a typical route [2]. Briefly, 0.50 g Vulcan XC 72 carbon (Cabot-Corp) was added in 100 mL of HNO_3 (65%; PanReac AppliChem) and the mixture was heated at reflux at 80 °C for 6 h. After reflux, the suspension was filtered, washed with plenty of Milli-Q water, and the obtained material was dried at 78 °C. In the second treatment, 0.50 g of Vulcan XC 72 was weighed and transferred to an alumina boat. The material was treated in a tubular furnace (model FT 1300/H, INTI) at 950 °C (5 °C/min) for 30 min, under a NH_3 (99.9999%; White Martins) atmosphere and a gas flow of 50 mL/min; and then, the support was cooled down to room temperature (the rate of 10 °C/min) [4]. The third nitrogenating treatment consisted of a combination of the first two procedures; the N-doped carbon was as described in treatment 1 followed by treatment 2.

In the second step, suitable amounts of tungsten oxide VI (WO_3) and synthesized N-doped carbons (CN) were added in 300 and 100 mL of an hydroalcoholic solution (60% ethanol in water, *v*/*v*), respectively. The solutions were maintained separately in an ultrasonic bath for 1 h, and later mixed and kept in an ultrasonic bath for another 2 h. After impregnation of precursors, the solvent was evaporated at 90 °C and the resulting powder was macerated and carburized, as described in the literature [23]. For carburization of WO_3, the obtained powders were transferred to an alumina boat, placed in a quartz tube, and treated in a tubular furnace, which was heated using a ramp of 50 °C/min until reaching 850 °C and remaining at this temperature for 4 h under an CH_4/H_2 atmosphere, 1:1 in volume (99,999%; White Martins), under a flow of 80 mL/min. The obtained material was cooled down to room temperature and passivated in a stream of 1 vol% O_2/Ar for 12 h at 25 °C. All tungsten carbide/N-doped carbons were synthesized to contain 30 wt.% of WC:C, since at this W/C content, the higher electrochemical performance for ORR of in alkaline medium was reported [16]. Synthesized supports prepared by treatments 1, 2, and 3 (see Fig. 1) were designated here as WC@CN-HNO_3, WC@CN-NH_3, and WC@CN-HNO_3-NH_3, respectively.

Synthesis of the Catalysts

The three types of synthesized supports were used to obtain six catalysts, according to the description below and illustrations in Fig. 1b, c. Firstly, the cationic complex $[Fe(TPTZ)_2]^{2+}$ was synthesized by a procedure already described in the literature [24], using as nitrogen and metal ion sources the precursors 2,4,6-Tris(2-pyridyl)-1,3,5-triazine (TPTZ; ≥ 99%,) and $(NH_4)_2$ $Fe(SO_4)_2.6H_2O$ (≥ 99%), respectively. Initial solutions were a mixture of 3.3×10^{-3} mol/L of the binder (TPTZ) solubilized in 20.0 mL of 60/40% vol. of an hydroalcoholic solution, where 3.0 mL of 0.2 mol/L of HCl was used to facilitating the solubilization of the binder. In another container 0.05 mol/L of the iron precursor salt $(NH_4)_2$ $Fe(SO_4)_2$ $6H_2O$ was solubilized in 300 mL of Milli-Q (18.2 MΩ/cm) water, maintaining the relation Fe:TPTZ in 1:2.1. The solution of ferrous salt (colorless) was added to the ligand solution immediately after the change of coloration to violet, indicating the formation of the complex ion $[Fe(TPTZ)_2]^{2+}$, which was maintained under magnetic stirring for 2 h.

After preparing the $[Fe(TPTZ)_2]^{2+}$ complex solution, the support was added in a proportion of 1.00 g of tungsten carbide/N-doped carbons to 5 wt.% Fe, and maintained under

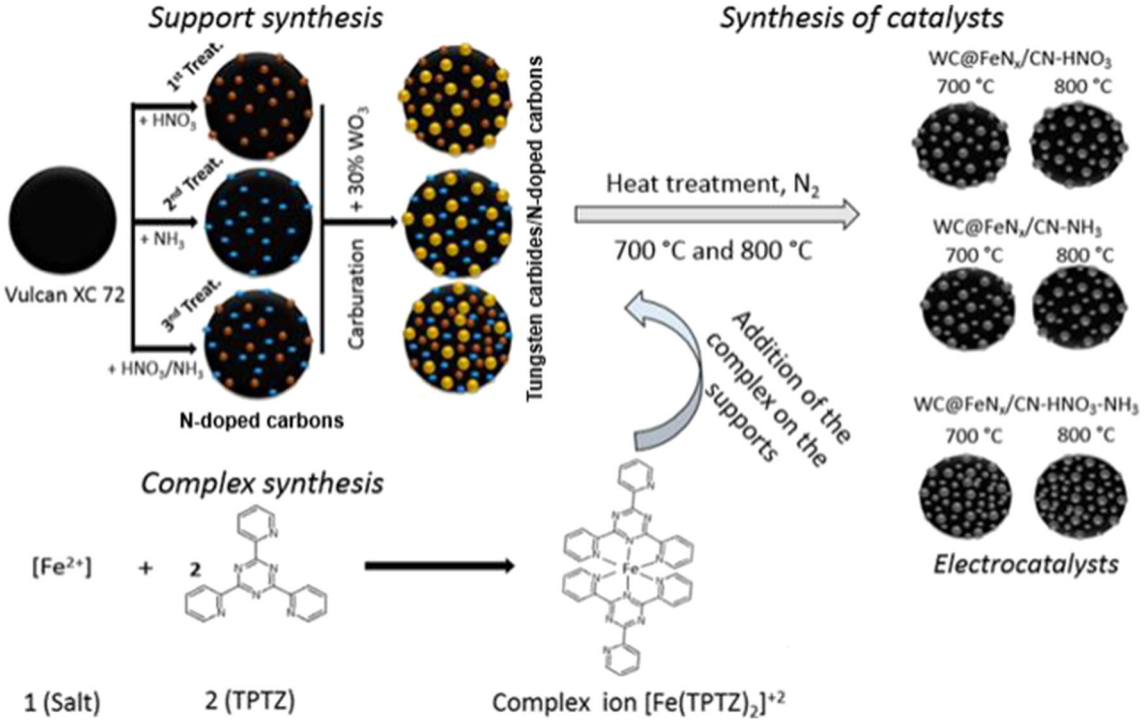

Fig. 1 Schematic illustration of the synthesis processes subdivided into steps, where **a** refers to the synthesis of the N-doped carbons and tungsten carbide/N-doped carbons, **b** refers to the preparation of the iron complex $[Fe(TPTZ)_2]^{2+}$, and **c** refers to the synthesis of the hybrid electrocatalysts

mechanical stirring for 24 h. Then, the suspension was left at 80 °C in a thermostatic bath for solvent evaporation. The dry powder was transferred to an alumina boat and placed in a quartz tube in a tubular furnace for the pyrolytic treatment. Before start heating, the system was saturated with N_2 with a flow of 130 mL/min for 10 min; after this period and under the same N_2 flow, the temperature was raised at a rate of 5 °C/min up to the final temperature (700 or 800 °C), remaining there for 2 h. Finally, the system was cooled down to room temperature. The synthesized catalysts were named here as $WC@FeN_x/CN\text{-}HNO_3(700)$, $WC@FeN_x/CN\text{-}HNO_3(800)$, $WC@FeN_x/CN\text{-}NH_3(700)$, $WC@FeN_x/CN\text{-}NH_3(800)$, $WC@FeN_x/CN\text{-}HNO_3\text{-}NH_3(700)$, and $WC@FeN_x/CN\text{-}HNO_3\text{-}NH_3(800)$. All reagents used in this work were analytical grade, without further purification, and solutions/washings were performed using purified Milli-Q (18.2 MΩ/cm) water.

Physical Characterizations

The structures of the synthesized catalyst powders were determined by XRD in a Rigaku Rotaflex® (model Ru200B) diffractometer, operating at 40 kV/40 mA, source of Cu:λ.Kα = 15,406 Å, in the range 10 °C to 90° (2θ) with a scanning speed of 1°/min. To determine the degree of graphitization of tungsten carbide/N-doped carbons and electrocatalysts, a Raman spectrometer, model T64000 from a Scientific HORIBA, with CCD detector cooled in liquid N_2 with a resolution of 2 cm was employed. All Raman signals were recorded in a spectral range of 1000–1800 cm. The elemental analysis was performed by EDX using LINK ANALYTICAL (Isis System Series 200) EDX equipment, with SiLiPentafe detector, coupled to an Electronic Microscope (ZEISS LEO 440 (Cambridge, England)). TEM analyses were realized in a JEOL-JEM2100 microscope at 200 kV. The oxidation states of the elements W, Fe, N, O, and C were determined by XPS using a K-alpha X-ray XPS system (Thermo Scientific), micro-focused Al-Kα X-ray source of 1486.6 eV, and a 180° focusing hemispherical analyzer 128-channel detector. The XPS results were adjusted using a Gaussian-Lorentzian function and Shirley background, and the catalyst binding energies were calibrated taking the carbon peak (C 1s) at 284.8 eV as reference.

Electrochemical Characterizations

The electrocatalytic activity of the catalysts for the ORR was evaluated in a three-electrode electrochemical cell, using a Pine Instrument (AUTOLAB-PGSTAT 30) bipotentiostat. A reversible hydrogen electrode (RHE) and a gold plate, 2 cm^2 of area, were used as reference and counterelectrodes, respectively. A rotating ring-disk electrode (RRDE; Pine Instruments, AFE6R1AU), composed by a gold ring and a glassy carbon disk, with a geometric area of 0.196 cm^2, to which a film of the catalysts was prepared by dropping a suspension of the corresponding material, was employed as

working electrode. The catalytic suspension was prepared from mixtures of 13.0 mg of the material, 2 mL of isopropyl alcohol (Sigma-Aldrich, ≥ 99%), and 30 μL of Nafion solution® (5% Nafion® in Isopropanol; Sigma-Aldrich), and left in an ultrasonic bath for 1 h until complete homogenization. Aliquots of 3 and 30 μL were added on the electrode surface, corresponding to a catalyst loading of 0.10 and 1.0 mg_{cat}/cm^2_{disk}, respectively. The electrolytes used in the electrochemical measurements were a 0.5 mol/L of H_2SO_4 solution and a 0.1 mol/L NaOH solution, saturated either with O_2 or Ar (both White Martins; 99.999%) according to the experiment. The temperature was maintained at 25.0 ± 0.1 °C by a flow of water along the jacket of the electrochemical cell, whose temperature was controlled by a Cole-Parmer thermostat. Cyclic voltammetry in an Ar-saturated electrolyte was used for the characterization of non-faradaic and faradaic processes related to specific characteristics of the surface chemical composition of the catalysts. For studies of the catalytic activity of the different catalysts against the ORR, the electrolyte was saturated with pure oxygen and the scanning rate of the working electrode potential was 1 mV/s. The ring was polarized at 1.5 V vs RHE for the determination of the amount of hydrogen peroxide produced during the ORR in the disk. The number of transferred electrons and the percentage of hydrogen peroxide produced were obtained using the RRDE measurements and Eqs. (1) and (2), respectively [19].

$$n = 4I_D/(I_D + (I_R/N)) \quad (1)$$

$$\%H_2O_2 = 100(4-n)/2 \quad (2)$$

where i_D and i_R are the disk and ring currents and N is the ring collection efficiency ($N = 0.36$) [25].

Stability tests were conducted as described in reference [26]. A polarization curve with a scanning rate of 1 mV/s and a rotating velocity of 400 rpm was performed for the ORR, after saturation with O_2 for 30 min. Then, the system was saturated with argon for 30 min and 5000 cycles of cyclic voltammetry (CV) between 0.60 and 1.0 V (vs RHE) were performed to evaluate the catalyst stability. At the end, a new ORR polarization curve was obtained, under the same conditions.

Results and Discussion

Physical Characterization

The chemical composition of the catalysts was first analyzed by EDX. The results (Table S1) show that the catalysts initially treated with NH_3 present lower mass/mass percentage of Fe. In all other cases, within the sensitivity of the EDX technique, results indicate that the Fe contents are reasonably closed to the nominal value (5 wt.%). The large deviation seen for WC@FeN_x/CN-NH_3(800) can be considered an exception, but the causes of the event is still unclear.

XRD, Raman, TEM, EDX, and XPS analyses were performed to further investigate the composition, structures, and morphologies of the synthesized materials. Figure 2a shows the diffraction patterns of the tungsten carbide/N-doped carbons. Firstly, it is important to note that the diffractograms of the tungsten carbide/N-doped carbons exhibited a shoulder at 25° (2θ), which refers to the (002) plane of the hexagonal carbon black structure [16, 27–31]. In addition, diffraction patterns related to the hexagonal phase of the tungsten carbides (WC; PDF# 89–2727) were also observed for these materials (Fig. 2), with intense and sharp peaks indicative of high WC crystallinity [13, 16, 32]. It is notable that there are no significant changes in the carbide XRD peaks caused by the three different types of N-doping carbon protocols.

Figure 2b shows the diffraction patterns of the hybrid FeN_x-containing catalysts synthesized under various pyrolysis

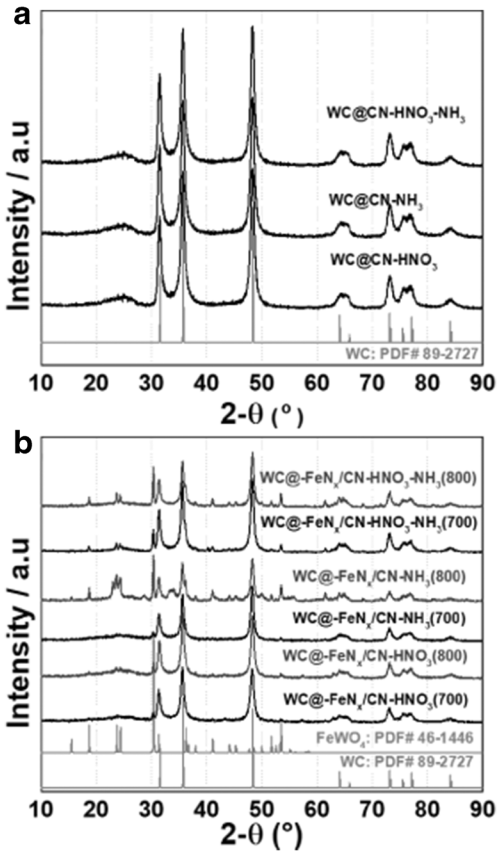

Fig. 2 **a** X-ray diffraction patterns of the synthesized tungsten carbide/N-doped carbons WC@CN-HNO_3, WC@CN-NH_3, and WC@CN-HNO_3-NH_3, together with the WC standard XRD pattern (PDF# 89–2727). **b** X-ray diffraction patterns of WC@-FeN_x/CN-HNO_3(700), WC@-FeN_x/CN-HNO_3(800), WC@-FeN_x/CN-NH_3(700), WC@-FeN_x/CN-NH_3(800), WC@-FeN_x/CN-HNO_3-NH_3(700), and WC@-FeN_x/CN-HNO_3-NH_3(800), together with the XRD patterns for ferberite standard ($FeWO_4$: PDF# 46–1446) and the WC standard (PDF# 89–2727)

temperatures, together with the patterns of WC (PDF# 89–2727 [13, 16, 32]) and ferberite ($FeWO_4$; PDF# 46–1446 [31]) standards. The presence of these two phases in the prepared materials is clearly denoted by these results, with the formation of ferberite ($FeWO_4$) being somewhat higher for those materials treated at 800 °C, as reported previously [16]. Estimations of the crystallite sizes of WC and $FeWO_4$ species were performed using the Scherrer equation, as shown in Table S2 [33]. Results show that the WC crystallite sizes in the supports (WC@CN-HNO_3, WC@CN-NH_3, WC@CN-HNO_3-NH_3) are in the range from 12 to 15 nm, which is essentially the same as for tungsten carbide prepared from bare carbon [16]. During the incorporation of the Fe-N_x species, there is a tendency of increasing the crystallite sizes of WC, reaching 15–20 nm in these materials, but no clear relationship between the pyrolysis temperature and the WC crystallite sizes could be established. The calculated $FeWO_4$ crystallite sizes were in the range of 40–45 nm.

Figure 3a–f illustrates TEM images of the Fe-N_x-based catalysts prepared at different pyrolysis temperatures, i.e., 700/800 °C. In these cases, images evidence that the N-doped carbon WC/C structure was similar to that reported previously for bare WC/C [12, 16], where differentiation between the WC and C phases was not possible due to the similarities in contrast of the constituent particles. On the other hand, images of the catalysts prepared with the NH_3-treated support evidenced the presence of rod/needle-type structures, distributed all over the catalyst sample (see also Figs. 3a–d and S2). These phases could have been formed by the growth of $FeWO_4$ structures, as directly evidenced by XRD data (Fig. 2). Formation of amorphous structures composed of H_xWO_3, as proposed previously [34] may be disregarded due to the clear crystalline aspect of the needles/rod observed in the images. Furthermore, the sizes of these rod/needle crystals (40–50 nm wide and 50–200 nm long) were compatible with the $FeWO_4$ crystallite sizes calculated from XDR data (Table S2). In the case of the HNO_3-treated carbon, the particles of ferberite present almost spherical shapes, while for the HNO_3-NH_3-treated sample the needle or spherical structures are less defined, but the presence of rod-shaped ferberite particles is still evident.

An important analytical technique used to characterize the degree of order/disorder of carbonaceous materials is the Raman spectroscopy [35]. Here, this technique was first used to investigate the graphitization of the carbon after the nitration steps with HNO_3, NH_3, and HNO_3-NH_3, and the incorporation of WC. Figure 4a, b shows the Raman spectra of the synthesized supports and catalysts, respectively. Peaks in the region 1344–1351 cm correspond to characteristic vibrations of sp^2-hybridized aromatic ring carbon atoms (D-band), while the peaks in the range 1585–1588 cm are attributed to the E_2g mode scattering by the elongation of the sp^2 hybridization of the carbons in the aromatic ring (G-band) [35, 36]. So, the integrated intensity ratio of these bands (I_D/I_G) has been used

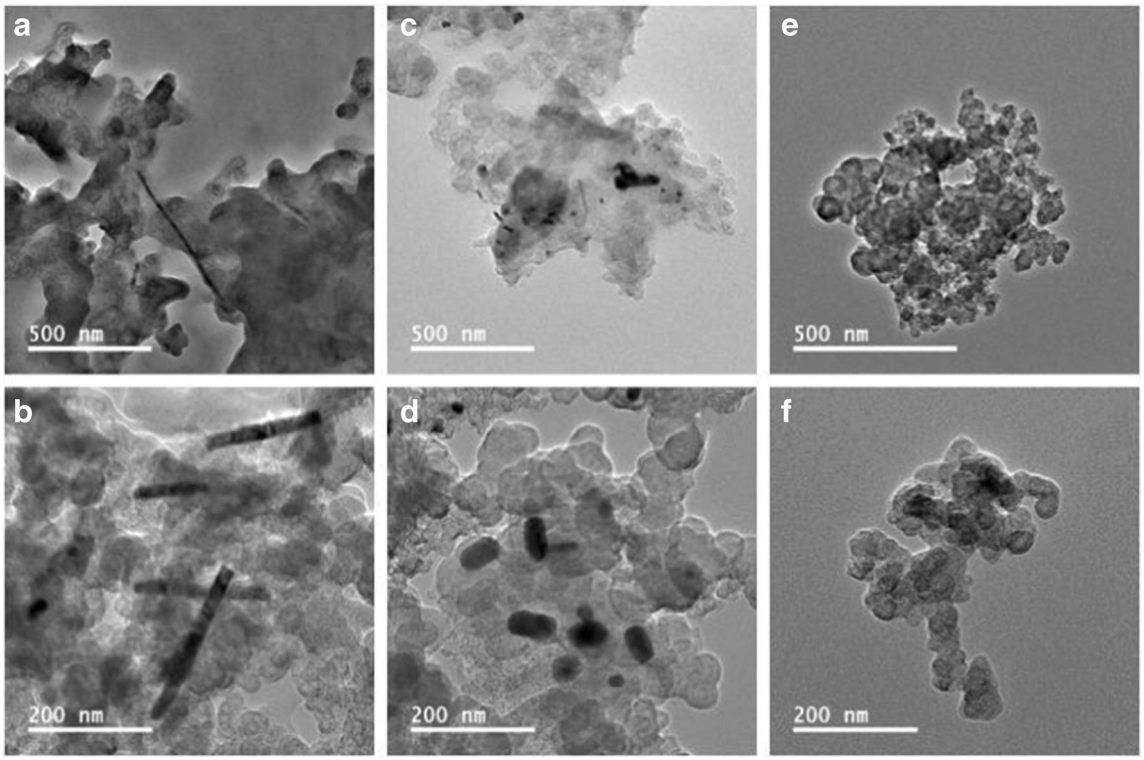

Fig. 3 TEM images of the Fe-N_x-containing catalysts at two magnifications. **a**, **b** WC@FeN_x/CN-NH_3(700). **c**, **d** WC@FeN_x/CN-HNO_3-NH_3(700). **e**, **f** WC@FeN_x/CN-HNO_3(800)

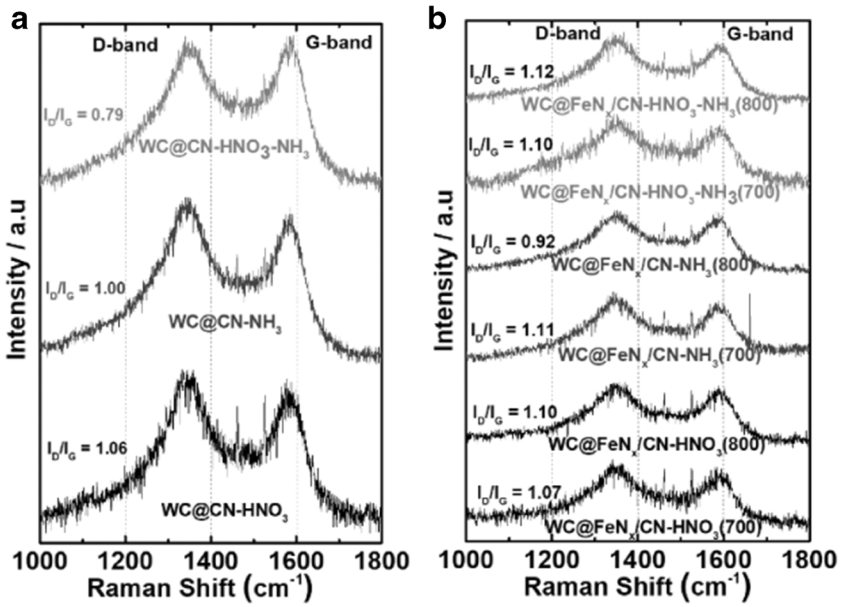

Fig. 4 Raman spectra of **a** the N-doped carbon substrates and **b** electrocatalysts prepared under different conditions

to evaluate the degree of defects in the structure of carbonaceous materials. The wave numbers of the D- and G-bands, together with the degrees of disorder of the materials, are provided in Table S3 [35, 37].

The data in Fig. 4 and Table S3 show that the nitration protocol resulted in changes in the degree of disorder of the carbon-based catalyst structures. The degree of disorder, which in the present cases comes from defects in the carbon structure after doping with N and/or incorporations of O, can be measured by the (I_D/I_G) ratio, that for tungsten carbide/N-doped carbon materials (Fig. 4a), follow the order WC@CN-HNO_3-NH_3 < WC@CN-NH_3 < WC@CN-HNO_3, indicating that ruptures of the graphitic networks were mainly caused by the treatments with nitric acid and ammonia.

Figure 4b shows the Raman spectra utilized to determine the degree of graphitization of the catalysts after incorporation of the FeN_x structures. The effects of the nitration procedure and the pyrolysis temperature may modify the structure of the carbonaceous materials, changing the degree of disorder [38]. The integrated intensity ratio (I_D/I_G; Table S3) suggest that the effect of nitration with HNO_3 on the degree of disorder was greater for catalysts treated at temperatures of 800 °C, while that for NH_3 is observed at 700 °C. The mixed HNO_3-NH_3 treatment resulted in high degrees of disorder at both temperatures. It can be noted that changes in the aromaticity disorder in the carbon atomic structures can be first caused by incorporation of nitrogen and or/oxygen atoms into the structure along the different initial carbon treatments. Addition of $[Fe(TPTZ)_2]^{2+}$ followed by the carburization of this composites (at 700 °C or 800 °C) may turn the understanding of the situation even more complex. This strongly challenges a systematization of the causes of the aromaticity disorder observed for the different final catalyst samples.

XPS was used to investigate the chemical composition and the oxidation states of the W, N, Fe, and C atoms, in the surface of the WC@FeN_x/CN-HNO_3(800), WC@FeN_x/CN-NH_3(700), and WC@FeN_x/CN-HNO_3-NH_3(700) catalyst nanoparticles, which presented higher electrochemical performances for the ORR (see the "Electrochemical Investigations of the ORR" section). Figure 5a shows the XPS survey spectra of these catalysts, while Table S4 presents the atomic compositions in terms of the W, N, Fe, C, and O components, as obtained from these analyses. The carbon treated with HNO_3-NH_3 presented a higher oxygen percentage (10.4%), as compared to values of 6.7% and 6.1% for the catalysts treated with only with HNO_3 or NH_3, respectively. This is in agreement with previous work, where it was found that in addition to nitrogen groups, treatment of carbon with HNO_3 and NH_3 species introduce oxygenated groups on the surfaces of the materials [1, 5]. Here, the balance of different trends regarding the incorporation of N or O in the materials evidences larger incorporation of O in WC@FeN_x/CN-HNO_3-NH_3(700) and larger introduction of N in the WC@FeN_x/CN-NH_3(700) catalyst.

Figure 5b–f shows the results for the deconvolution of the high-resolution XPS spectra of the electrocatalysts to give the W 4f, N 1s, Fe 2p, O 1s, and C 1s binding energies, respectively. For nitrogen (Fig. 5c), five peaks were fitted and these were assigned to the presence of N-pyridine, Fe-N_x, N-pyrrole, N-graphitic, and N-graphitic oxide species [39–42]. The N species with the higher percentages were the N-graphitic and N-pyridine types, considered to be active nitrogen centers for the ORR in acidic and alkaline media, respectively [16, 43, 44]. The total nitrogen content was found to be highest for the HNO_3 treatment (1.9%), followed by the NH_3 (1.3%) and the

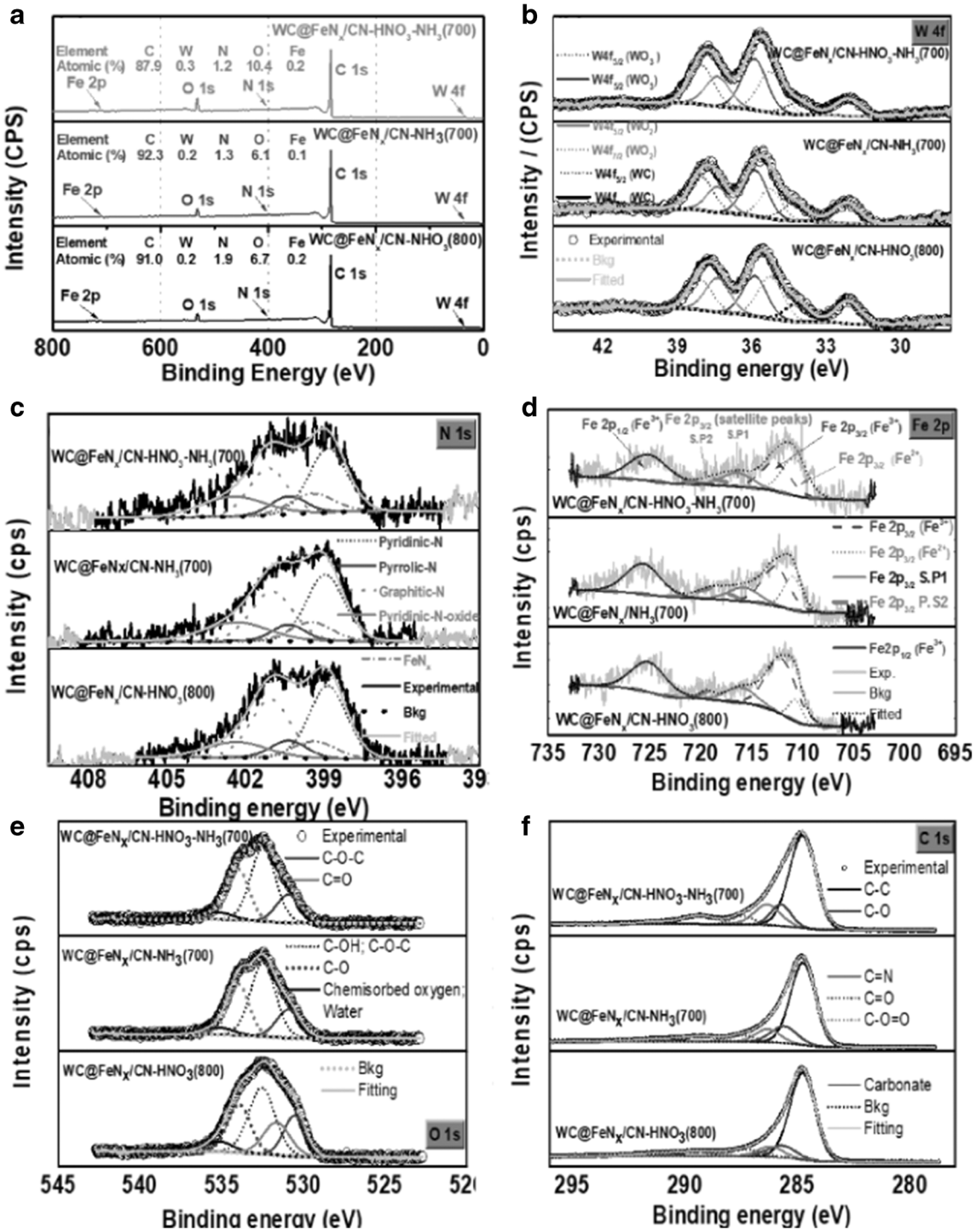

Fig. 5 X-ray photoelectron spectroscopy (XPS) spectra of the WC@-FeN_x/CN-HNO_3(800), WC@-FeN_x/CN-NH_3(700), and WC@-FeN_x/CN-HNO_3-NH_3(700) electrocatalysts. **a** Wide scan spectrum. **b** High-resolution W4f spectrum with peaks deconvoluted into WC, WO_2, and WO_3. **c** High-resolution N 1s spectrum with the peaks deconvoluted into pyridinic, pyrrolic, graphitic/quaternary, and pyridinic-oxidized nitrogen species. **d** High-resolution Fe 2p spectrum with peaks deconvoluted into Fe^{2+} and Fe^{3+} species. **e** High-resolution O 1s spectrum. **f** High-resolution C 1s spectrum

HNO_3-NH_3 (1.2%) treatments. Correlations considering the contents of nitrogen species, pH, and catalytic activity are discussed in the "Electrochemical Investigations of the ORR" section.

In the case of tungsten, the spectra were deconvoluted into six well-defined peaks for the three electrocatalysts investigated (Fig. 5b). The atomic percentages of the elements (Table S4) pointed to the presence of WO_3, WO_2, and WC

species. The large amount of tungsten oxides is probably partly related to the reaction of tungsten with oxidized iron species and/or water, so it could have been associated with the presence of ferberite ($FeWO_4$) [16, 44], as indicated by the XRD and TEM results. Figure 5d shows the deconvolutions of the XPS spectra for Fe 2p at low (Fe $2p_{3/2}$) and high-energy orbitals (Fe $2p_{1/2}$). The peak at approximately 710.7–710.8 eV

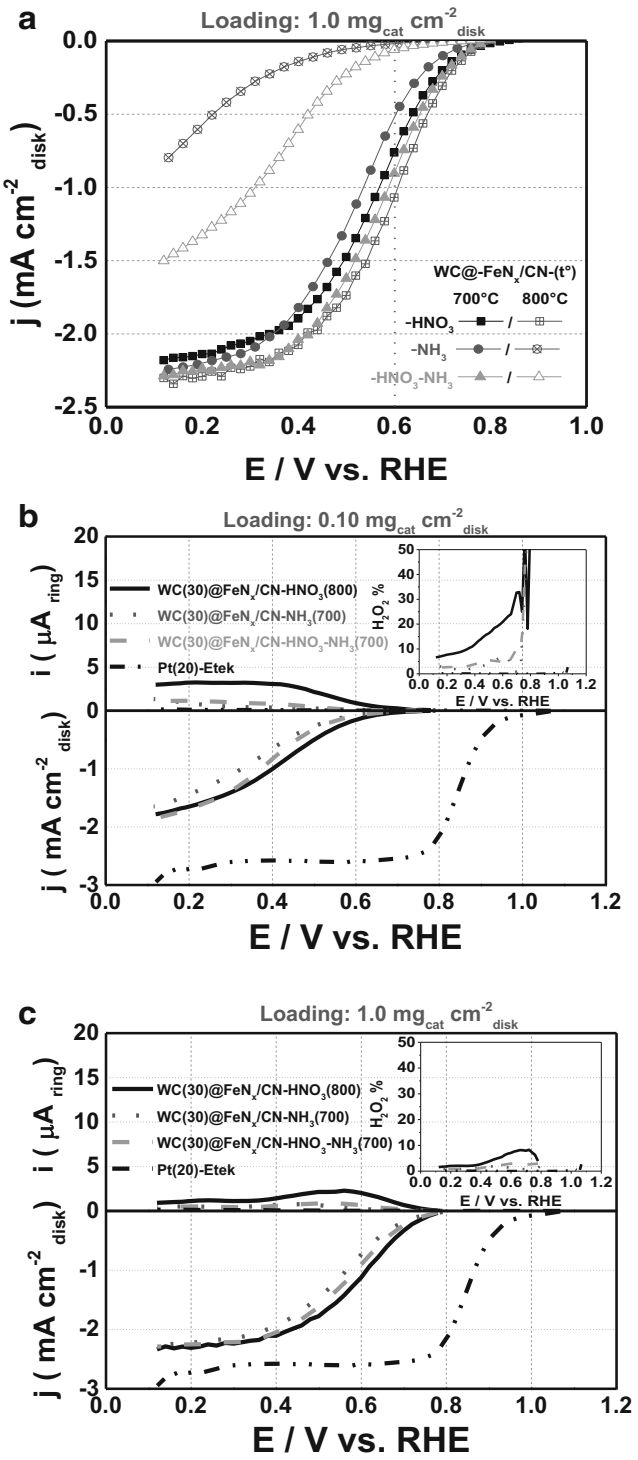

◀ **Fig. 6** **a** Polarization curves of the oxygen reduction reaction on the WC@-FeN_x/CN-HNO_3(700), WC@-FeN_x/CN-HNO_3(800), WC@-FeN_x/CN-NH_3(700), WC@-FeN_x/CN-NH_3(800), WC@-FeN_x/CN-HNO_3-NH_3(700), and WC@-FeN_x/CN-HNO_3-NH_3(800) electrocatalysts in 0.50 mol/L of H_2SO_4, at a loading of 1.0 mg_{cat}/cm^2_{disk}. **b**, **c** Results of RRDE experiments to obtain the ORR polarization responses and corresponding hydrogen peroxide percentages for the best electrocatalysts of **a** WC@FeN_x/CN-HNO_3(800), WC@FeN_x/CN-NH_3(700), and WC@FeN_x/CN-HNO_3-NH_3(700) at a loading of **b** 0.10 mg_{cat}/cm^2_{disk} and **c** 1.0 mg_{cat}/cm^2_{disk}, compared to a 20 wt% Pt/C catalyst from E-TEK. RRDE experiments performed at a scan rate (v) of 1 mV/s and RRDE rotation rate (w) of 400 rpm in 0.50 mol/L of H_2SO_4 as electrolyte and with the temperature controlled at 25.0 ± 0.1 °C. RRDE disk electrode area of 0.196 cm^2

in the Fe $2p_{3/2}$ region was attributed to Fe^{2+} [44], possibly associated with FeO and $FeWO_4$. Two other peaks were also observed, at 712.7–712.8 eV (Fe $2p_{3/2}$) and 725.4–725.6 eV (Fe $2p_{1/2}$), associated with Fe^{3+}, suggesting the formation of the Fe-N_x structures, whose N-graphitic electrons are coordinated to Fe [45, 46]. Finally, satellite peaks present at 715.9–716.5 eV and 718.9–719.2 eV were associated with Fe^{2+} and Fe^{3+}, respectively [46–50].

In the case of oxygen (Fig. 5e), for the three electrocatalysts, the deconvolution resulted in four functional groups coherent with the presence of carbonates C–O–C (530.6–531.2 eV), carboxylate C–OH and C–O–C (532.4–532.6 eV), carboxylate C–O (533.9 eV), and adsorbed water (535.0–535.2 eV) for the three electrocatalysts [35, 51]. A specific band at 531.7 eV, corresponding to the C=O bond, appeared for the catalyst treated with HNO_3, suggesting the formation of an acid functional group [5].

Deconvolution of the XPS spectra for C 1s resulted in several peaks attributed to the sp^2 hybridization of carbon atoms (284.8 eV), the sp^2 hybridization of carbon in C=N (285.6–285.7 eV) bonding, and C–O (286.2–286.3 eV), C=O (287.2–287.4 eV), O–C=O (289.2–289.4 eV), and carbonate (2912–291.4 eV) species [35, 36]. The catalysts investigated had high carbon contents and C–C sp^2 hybridization values above 60% (Table S4), indicative of their suitable electronic conduction [52, 53], in agreement with the Raman data and the results of the electrochemical analyses.

Electrochemical Investigations of the ORR

The tungsten carbide/N-doped carbon supports were characterized by cyclic voltammetry in acid electrolyte (0.50 mol/L H_2SO_4) saturated with Ar or O_2 at 20 mV/s between 0.1 and 0.8 V vs RHE. The upper limit potential was restricted to 0.8 V to avoid any possibility of WC oxidation, as observed for non-doped WC/C catalysts [54, 55]. The results for the N-doped carbon WC/C supports in argon or oxygen atmospheres are shown in Fig. S2. The CV responses for these substrates in an Ar atmosphere indicated an absence of redox peaks at the two catalyst loadings used (0.10 and 1.00 mg_{cat}/cm^2_{disk}).

However, in the presence of oxygen, reduction currents were recorded for all materials, evidencing ORR catalytic activity in all cases. The magnitude of reduction currents and values of onset (E_o) for the ORR varied according to the nitration treatment, for both catalyst loadings, indicating following sequence regarding the activity for the ORR: HNO_3-NH_3 > HNO_3 > NH_3.

Figure 6a compares polarization curves for the oxygen reduction reaction in the H_2SO_4 electrolyte for WC/Fe-N_x-containing catalysts presenting different carbon doping degree/groups, prepared with different nitrogenous species (HNO_3, NH_3, and HNO_3-NH_3) and treated at different pyrolytic temperatures (700 and 800 °C). These results evidence higher ORR catalytic activity for the electrocatalysts pyrolyzed at 700 °C, as reported before for non-functionalized carbons [16]. An exception was the catalyst nitrided with only HNO_3, which presented better performance when treated at 800 °C. In the overall, the electrocatalytic activities of the materials in acidic media follow the order: NH_3 (700 °C) < HNO_3-NH_3 (700 °C) < HNO_3 (800 °C), with half-wave potentials at 0.515 V, 0.570 V, and 0.592 V vs RHE, respectively, at a loading of 1.0 mg_{cat}/cm^2. This order approximately followed those of nitrogen, iron, and Fe-N contents in these catalysts, as measured by XPS (Table S4). This is consistent with the presence of the Fe–N–C structures that are reported to be the most activity centers for the ORR in acid media [56]. Here, it is also noted that there is a tendency of a decrease in the ORR activity with the increase of the crystallite size of ferberite. However, this happens in parallel with the effect of other synthesis parameters, e.g., nitration of carbon and formation of surface species, which may make a discussion around the ORR activity as due exclusively to ferberite not solidly grounded.

In the WC/Fe-N_x-containing materials, the contents of WC in the catalyst particle surfaces are of the order of 10 at.%, with the rest being WO_x, as evidenced by XPS (Table S4). All these components are featureless in the potential ranges used here for the ORR investigation, as evidenced by the absence of redox features in the results of Figs. 6 and 7. The results also indicated that the most promising electrocatalysts for reducing oxygen, in terms of mass activity (RRDEs presenting the same mass of materials), were WC@FeN_x/CN-HNO_3(800), WC@FeN_x/CN-NH_3(700), and WC@FeN_x/CN-HNO_3-NH_3(700). Finally, it is noteworthy that further increasing the pyrolysis temperature did not enhanced the ORR activity on the electrocatalysts, as illustrated in Fig. S3.

These more active selected electrocatalysts were further investigated using different loadings, in the presence or absence of Fe, and these results obtained by using the RRDE technique are shown in Fig. 6b, c. It is seen that an increase of the non-precious metal catalyst loading on the disk of the RRDE electrode (see Fig. 6b, c) was accompanied by an increase of the oxygen reduction currents and a decrease of the

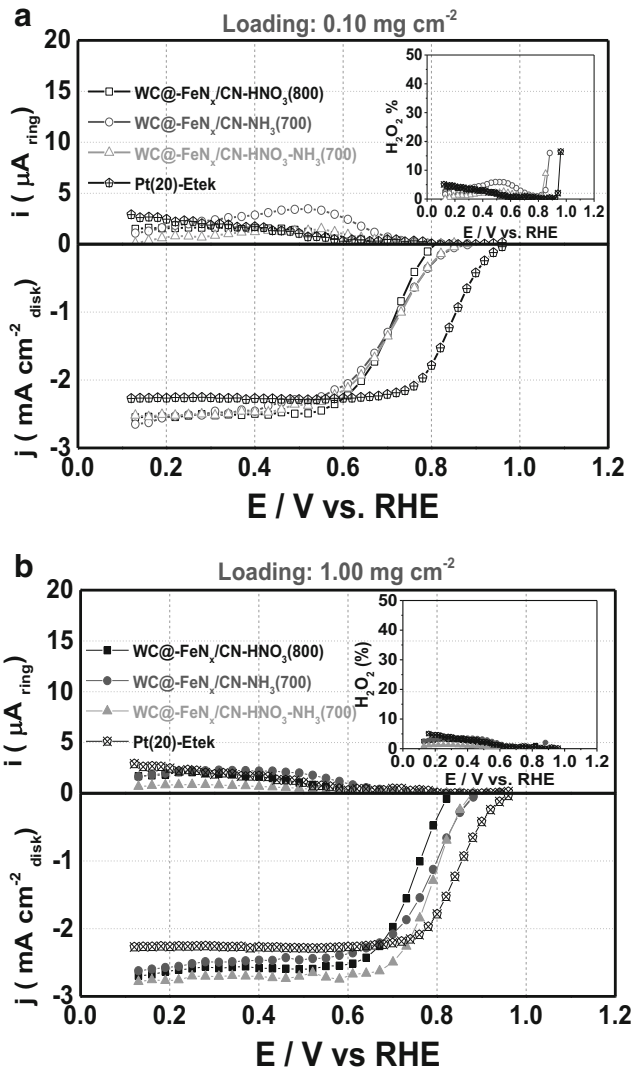

Fig. 7 RRDE oxygen reduction reaction polarization responses on the disk and corresponding hydrogen peroxide oxidation on the ring for the catalysts: WC@FeN_x/CN-HNO_3(800), WC@FeN_x/CN-NH_3(700), and WC@FeN_x/CN-HNO_3-NH_3(700) catalysts in alkaline electrolyte at catalyst loadings of **a** 0.10 mg_{cat}/cm^2_{disk} and **b** 1.0 mg_{cat}/cm^2_{disk} RRDE experiments performed at a scan rate (v) of 1 mV/s and RRDE rotation rate (w) of 400 rpm in 0.1 mol/L NaOH as electrolyte and with the temperature controlled at 25.0 ± 0.1 °C. RRDE disk electrode area of 0.196 cm^2

hydrogen peroxide oxidation currents. Another interesting trend was observed for the ring currents (insets Fig. 6b, c), which denote a decrease of the percentage of H_2O_2 at less positive potentials (reflecting lower extents of hydrogen peroxide reduction rates at E < ~0.7 V vs RHE).

Recently, Lopes et al. [57] has shown that the ORR on metal-N_x/C catalysts might proceed according to a $2e^-$ reduction mechanism to H_2O_2 at potentials less positive than ~0.75 V vs RHE, and according to a $4e^-$ reduction mechanism to H_2O at potentials more positive than ~0.75 V vs RHE. As pointed out by Choi et al. [58], the extent of the reduction of H_2O_2 to water on metal-N_x/C catalysts is related to the

effectiveness of the transport of H_2O_2 away through the catalyst layer. This means that at high catalyst loadings, there is a higher probability of the H_2O_2 being reduced to water. These features were in agreement with the ORR on the non-precious metal catalysts synthesized in this work, as shown in Fig. 6b, c. Therefore, in acidic media, the oxygen reduction reaction on the catalysts presented in Fig. 6 seems to proceed by means of a $2e^- + 2e^-$ reduction mechanism within the potential window studied. As shown recently for this class of catalysts without carbon nitration [16], the activity of WC/WO_x catalysts for the ORR in acid media is not so high, but it is effectively not negligible in the potential range where the reaction takes place in the $WC@FeN_x$ nitride materials (Fig. 6b, c). In this way in acidic media is likely here the reaction first involves a reduction of oxygen to hydrogen peroxide on both

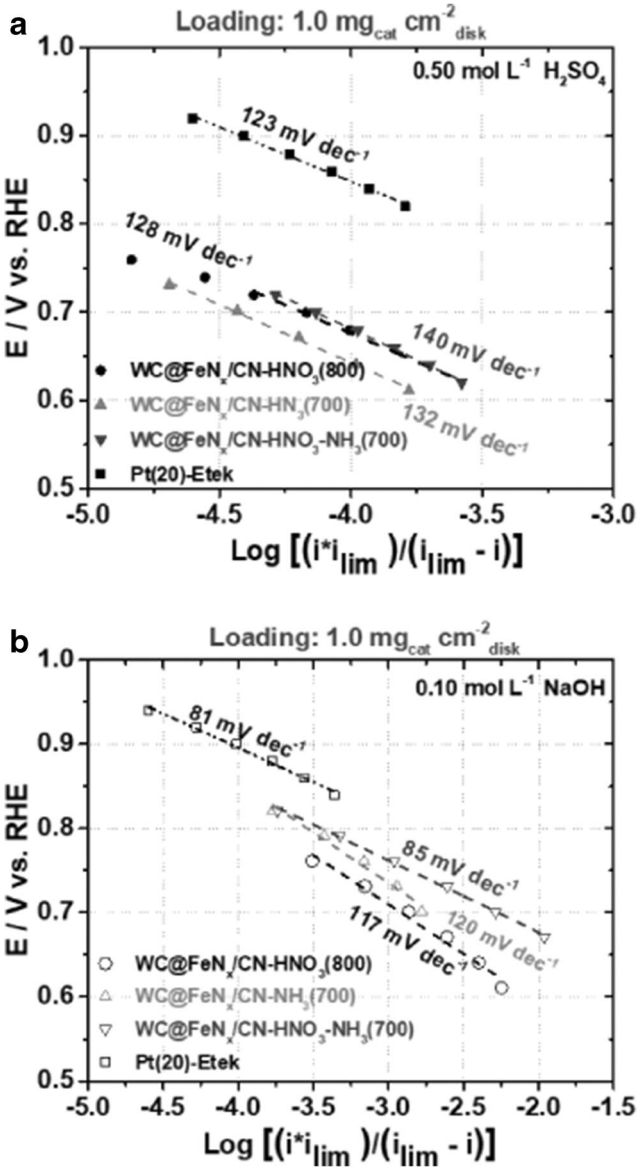

Fig. 8 Mass-transport corrected Tafel plots for the ORR on selected catalyst at high catalyst loadings in **a** acid and **b** alkaline media

active sites (WC and FeN_x), followed by a second reduction reaction of peroxide to water on FeN_x sites. This is also coherent with the recent observation that in acid media WC reduces oxygen to H_2O_2 and that N/C sites are protonated and inactive in acidic media [58]. In summary, at the higher catalyst loading, there is a substantial decrease of hydrogen peroxide formation, showing that under this condition, the thickness of the layer could determine both the catalytic activity and the reaction mechanism, by providing a greater number of active sites and a longer residence time during which the H_2O_2 reduction could take place [16, 57].

The role of the metal in the structure of metal-N/C electrocatalysts is a matter of ongoing discussion. Two possibilities have been reported for the role of the transition metal iron. The first one is that the active site is formed by Fe-N_4/C and Fe-N_2/C structures [59, 60]. The other possibility is that during the heat treatment the metal catalyzes the formation of active sites, but it is not part of the active site [59, 60]. To investigate such behavior, the three best electrocatalysts were prepared with a nitrogen chelating group (TPTZ; see the "Synthesis of the Catalysts" section), in the absence of iron. The scheme of the synthesis is shown in Fig. S4, while the results of EDX analyses, confirming the absence of this metal, are presented in Table S5. The electrochemical responses of these materials towards the ORR at high catalyst loadings (1.00 mg_{cat}/cm^2_{disk}) in acid medium (0.5 mol/L of H_2SO_4) are shown in Fig. S5. It is seen that the three catalysts show reduced catalytic activities that were well below those of the catalysts with iron at the same loading (Fig. 6). These results, together with literature data [3, 19, 22, 61], indicate that iron is fundamental in obtaining a significant ORR catalytic activity at low pHs. Importantly, comparison of the ORR polarization data for the catalysts prepared with iron (Fig. 6) and without iron (Fig. S5) evidence that the WC and N/C sites were far less active than FeN_x sites towards the ORR in acidic media, irrespectively of the type or content of surface species (see the XPS data in Table S4).

It is well known that hybrid electrocatalysts present different behaviors in acid and alkaline environments. Here, the most active electrocatalysts in acid electrolyte, $WC@FeN_x/CN\text{-}HNO_3(800)$, $WC@FeN_x/CN\text{-}NH_3(700)$, and $WC@FeN_x/CN\text{-}HNO_3\text{-}NH_3(700)$, were also investigated in terms of their ORR activities in alkaline media 0.1 mol/L of NaOH. The polarization curves (Fig. 7) show that compared to the results obtained in acid, at high pH, there was a lower effect of the catalyst loading on the ORR. The reaction onset potentials (for a catalyst loading of 1.00 mg_{cat}/cm^2_{disk}) were higher in alkaline medium and located at 0.82, 0.88, and 0.88 V vs RHE for $WC@FeN_x/CN\text{-}HNO_3(800)$, $WC@FeN_x/CN\text{-}NH_3(700)$, and $WC@FeN_x/CN\text{-}HNO_3\text{-}NH_3(700)$, respectively, with no correlation with the nitrogen or iron contents of the samples (Table S4). It was recently shown [16] that WC is suitably active for reducing oxygen

Table 1 Electrochemical parameters for the ORR on selected catalysts at a loading of 1.00 mg_{cat}/cm^2_{disk} at a potential of 0.7 V vs RHE in acid and alkaline media

Catalyst	Number of electrons $n = \frac{\lvert 4i_D \rvert}{\lvert i_D \rvert + (i_R/N)}$	Percentage of H_2O_2 (%) $H_2O_2(\%) = 100\left(\frac{\frac{2i_R}{N}}{\lvert i_D \rvert + \left(\frac{i_R}{N}\right)}\right)$	Tafel (mV/dec) $\text{Log} = \left[\frac{(i \times i_D)}{(i_D - i)}\right]$
H_2SO_4 (0.5 mol/L)			
WC@FeN_x/CN-HNO_3(800)	3.98	0.93	128
WC@FeN_x/CN-NH_3(700)	3.99	0.46	132
WC@FeN_x/CN-HNO_3-NH_3(700)	3.98	1.19	140
Pt/C(20)-Etek	3.99	0.30	123
NaOH (0.1 mol/L)			
WC@FeN_x/CN-HNO_3(800)	4.00	0.11	117
WC@FeN_x/CN-NH_3(700)	3.99	0.32	120
WC@FeN_x/CN-HNO_3-NH_3(700)	4.00	0.07	85
Pt/C(20)-Etek	3.99	0.21	81

to hydrogen peroxide in alkaline media. Furthermore, Liu et al. [62] showed that the catalytic activity of N/C sites towards the ORR in alkaline media follows the order pyridinic-N > pyrrolic-N > graphitic-N > oxidized-N. In addition, Malko and Kucernak [63] have proposed a significant outer sphere electron transfer component for the ORR on Fe-N/C catalysts in alkaline media. From these findings, together with the XPS data (Table S4) and the ORR results (Fig. 7), it is apparent that the oxygen reduction reaction on iron-containing catalysts in alkaline media depends on many active sites and mechanisms of similar importance.

Insets in Fig. 7a, b show the percentage of H_2O_2 generated in the ORR on the selected catalysts demonstrating the little variation in the formation of this species at different catalyst loadings. Along with the limiting currents (similar to that of Pt/C), results denote that these electrocatalysts reduce oxygen predominately to water in alkaline electrolyte, in agreement with literature findings [22]. Figure S6 shows the ORR electrochemical response of selected electrocatalysts synthesized in the absence of iron at two catalyst loadings of 0.10 mg_{cat}/cm^2_{disk} and 1.00 mg_{cat}/cm^2_{disk}, in alkaline electrolyte (0.1 mol/L NaOH). In contrast to the data obtained in acid medium (Fig. S5), the electrocatalysts prepared without iron were significantly active towards the ORR in alkaline media. Results for the catalysts without iron in the structures containing nitrogen species provide three important information. Firstly, their high catalytic activities at the two loadings (with similar onset potentials, above 0.8 V vs RHE) evidenced the important role of the N/C and WC structures for the ORR [16, 56, 57]. However, since the activities of the electrocatalysts with iron are still higher than those without iron, other active sites, besides WC and N/C, were likely to exist in the presence of this metal [56]. These were probably associated with Fe-N_x sites by means of an outer sphere electron transfer process [63], given that OH^- ions are strongly bound to the iron center in Fe-N_x sites in alkaline media [56]. The second point is that at 0.1 mg_{cat}/cm^2, the ORR curves of the electrocatalysts did not seem to steadily reach the theoretical limit current for the $4e^-$ mechanism. The third point is that the ORR on the catalysts prepared in the absence of iron produced high ring oxidation currents (~40 H_2O_2% at 0.5 V vs RHE; inset to Fig. S6a). These results suggested that a higher content of N was not enough to result in an ORR activity comparable to the activities of electrocatalysts containing iron in their structure, even at high loadings (Fig. S6b). Furthermore, from comparison of the data for the catalysts prepared with (Fig. 7) and without iron (Fig. S6), it turns evident that the iron-containing catalysts reduce oxygen predominantly to OH^- in alkaline media, at potentials below ~0.7 V vs RHE. On the other hand, catalysts prepared without iron reduced oxygen predominantly to H_2O_2 at this pH (Fig. S5a) and in the same potential region.

Figure 8 shows Tafel lines for the oxygen reduction reaction on different catalysts in acid and alkaline media, plotted after correcting the current densities for mass transport processes [19]. The results shown in Fig. 8a clearly evidences the much lower ORR activities of the Fe-N_x-containing materials, in acid media compared to Pt/C. In contrast, the results shown in Fig. 8b revealed the significantly improved activities of the same materials in the alkaline electrolyte. Table 1 summarizes the obtained values of Tafel slopes for the ORR ion the WC@FeN_x/CN-HNO_3(800), WC@FeN_x/CN-NH_3(700), and WC@FeN_x/CN-HNO_3-NH_3(700) electrocatalysts at high loadings in acid and alkaline electrolytes. Data related to the number of electrons (n) obtained at 0.7 V and using Eq. (1) and the percentage of hydrogen peroxide (%H_2O_2) are also included.

Tafel coefficient values (Table 1) of ~128 mV, ~132 mV, and ~140 mV/dec (acid medium) and ~117, ~120, and ~85 mV/dec (alkaline medium) were calculated for the ORR on the WC@FeN_x/CN-HNO_3(800), WC@FeN_x/CN-NH_3(700), and WC@FeN_x/CN-HNO_3-NH_3(700) catalysts,

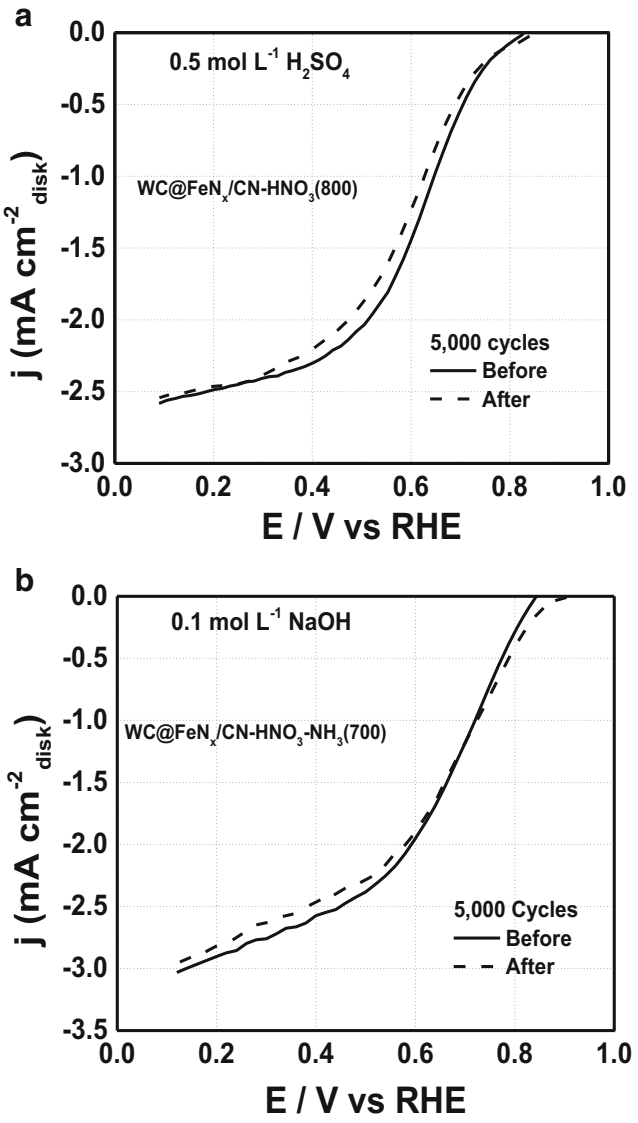

Fig. 9 Oxygen reduction reaction polarization curves obtained before and after the potential cycling durability tests for the catalysts **a** WC@FeN_x/CN-HNO_3(800) in 0.5 mol/L H_2SO_4 and **b** WC@FeN_x/CN-HNO_3-NH_3(700) in 0.1 mol/L NaOH. Catalyst loading: 2.0 mg_{cat}/cm^2_{disk}. Oxygen reduction reaction polarization curves performed at a scan rate (v) of 1 mV/s and RRDE rotation rate (w) of 400 rpm in electrolytes with the temperature controlled at 25.0 ± 0.1 °C. RRDE disk electrode area of 0.196 cm^2

respectively. These values are in the same range as those observed for platinum catalysts (120 mV/dec) at potentials where the electrode surface presents low coverages of oxygenated reaction intermediate species on Pt [39]. This similarity might indicate the occurrence of similar reaction mechanisms and/or reaction order, and rate determining steps on both types of electrodes in acid or alkaline electrolytes, at least when nitrogen-doped Fe-N_x-containing catalysts are considered [39, 57]. On the other hand, results in Table 1 show values of n close to 4 for the ORR on the selected catalysts. This was consistent with the low levels of hydrogen peroxide measured at 0.7 V vs RHE (Figs. 6c and 7) and with the earlier findings of Lopes et al. that FeN_x/C catalysts reduced oxygen to water at potentials above ~0.75 V vs RHE (note that this potential varies with temperature and with the concentration H_2O_2 near the active sites [57]).

Stability Tests of the Best Electrocatalysts

For an electrocatalyst to be considered viable for practical applications, it must present suitable catalytic activity and remain stable for an extended period of time. Here, a preliminary investigation of the electrocatalyst stability was performed with the most representative materials in acid (WC@FeN_x/CN-HNO_3(800)) and alkaline (WC@FeN_x/CN-HNO_3-NH_3(700)) electrolytes. The electrodes were cycled between 0.6 and 1.0 V (vs RHE) at a scan rate of 50 mV/s, for 5000 cycles in acid or alkaline electrolytes, following a testing protocol described in the literature [26]. Despite that oxygen-saturated electrolytes offer a broader perspective, the aging text conducted here was made in absence of oxygen. We consider that these results is valid as an initial approach for separating the effect of electrode potential from those related to the presence of O_2, particularly regarding the corrosion of carbon on the Fe–N–C active sites in acidic media and on WC and C–N species in alkaline media.

Figure 9 shows the ORR polarization results obtained before and after the durability test in acid and alkaline electrolytes. Suitable performance and stability were evidenced by small differences in the ORR polarization curves before and after the potential cycling. This indicated that these electrocatalysts could be considered promising for practical applications [64] due to their high catalytic activity and stability.

XPS analyses of the catalysts were performed before and after the durability tests in order to gain insights on the degradation process affecting their activity for the ORR. Table 2 presents the relative variation in the atomic composition of the materials after and before the durability tests of catalysts, as presented in Fig. 9. A clear trend in the XPS data is the increase in the relative oxygen content, loss of carbon, and oxidation of tungsten. Even though relatively significant, these changes have not significantly affected the ORR activity of the materials, in agreement with the fact that WC is less active than FeN_x/N-C moieties towards the ORR [16], given that there is an increase in the relative amount of the later compared to the former species after the durability test. Considering iron, data in Table 2 evidence a relative increase in the content of this element in both catalysts after the durability tests. This fact might be associated with the great loss of carbon, possibly through its oxidation to CO_2, which would increase the relative amount of other elements. Nevertheless, the appearance of an XPS peak relative to Fe–N suggests occurrence of such corrosion processes of the catalyst surface

Table 2 Relative variations in atomic compositions (%) after the durability tests of selected catalysts

	(+) i.e., increase in at%; (−) i.e., reduction in at%				
	Data from XPS survey scans				
	C 1s	O 1s	W 4f	N 1s	Fe 2p
WC@FeNx/CN-HNO_3(800) acidic media	− 9.1	+ 7.8	+ 1.0	− 0.6	+ 0.9
WC@FeNx/CN-HNO_3-NH_3(700) alkaline media	− 8.9	+ 8.5	+ 0.3	− 0.3	+ 0.4

Atomic composition (%) of W 4f, N 1s, Fe 2p, C 1s, and O 1s of the catalysts WC@FeN_x/CN-HNO_3(800) and WC@FeN_x/CN-HNO_3-NH_3(700) after and before the stability test, as determined by XPS analyses

leading to the exposure of more surface iron. This fact could explain the suitable stability of the catalyst activity in acidic media, whereas in alkaline media the relative increase in WC and C–N species, after the durability test (Table 2), could explain the stability of the catalyst, given that these species have been shown to be suitably active towards the ORR in this pH range in comparison to Fe–N species [16, 56, 63].

Conclusions

Tungsten carbide/N-doped carbons and iron-containing hybrid electrocatalysts were synthesized and evaluated as potential catalysts for the oxygen reduction reaction in both acid and alkaline media. The materials were thoroughly characterized by XRD, TEM, EDX, Raman spectroscopy, and XPS, in addition to cyclic voltammetry and ORR polarization response analyses using the RRDE technique. The performance of the best catalysts varied according to the type of nitration protocol, the presence of iron, and the heat treatment employed. The high performance of the synthesized electrocatalysts in an alkaline medium was demonstrated by only a 0.04-V difference in the ORR polarization response, relative the commercial ETEK Pt/C catalyst. The number of electrons transferred per oxygen molecule varied according to pH and catalysts, following different reduction mechanisms. In addition, in acid medium, the catalyst loading influences the type of reaction mechanism (from a $2e^-$ to a $2e^- + 2e^-$), with the presence of iron being essential in order to produce materials with high catalytic activity (at low pH) and selective (high pH) materials, indicating a strategy to increase the electrocatalyst performance. In an alkaline medium, iron also influenced (albeit to a lesser extent) the performance of the materials in catalyzing the ORR, with this metal being crucial in promoting a reduction mechanism towards OH^- and dramatically decreasing the formation of deleterious H_2O_2, compared to iron-free catalysts. Under a standard durability test protocol, the best electrocatalysts presented a reduced degradation and promising long-term stability for practical applications, where XPS data suggested corrosion of carbon leading to further exposure of ORR active sites, which would support the suitable longevity of the catalysts.

Funding The Coordenacao de Aperfeicoamento de Pessoal de Nivel Superior (CAPES; process number 1423454) and the Sao Paulo Research Foundation (FAPESP) under process number 2013/16930-7 provided the financial support. T.L. was provided support by the Sao Paulo Research Foundation under projects 14/22130-6 and 17/15304-6 for T.L.'s Young Investigator Award (i.e., research fellowship) and the support of project 2014/09087-4. T.L. was also provided support by the RCGI Research Centre for Gas Innovation, sponsored by FAPESP (2014/50279-4) and Shell.

References

1. H. Wang, R. Côté, G. Faubert, D. Guay, J.P. Dodelet, Effect of the Pre-Treatment of Carbon Black Supports on the Activity of Fe-Based Electrocatalysts for the Reduction of Oxygen. J. Phys. Chem. B **103**(12), 2042–2049 (1999)
2. T. Schilling, M. Bron, Oxygen reduction at Fe–N-modified multiwalled carbon nanotubes in acidic electrolyte. Electrochim. Acta **53**(16), 5379–5385 (2008)
3. M. Bron, J. Radnik, M. Fieber-erdmann, P. Bogdanoff, S. Fiechter, EXAFS, XPS and electrochemical studies on oxygen reduction catalysts obtained by heat treatment of iron phenanthroline complexes supported on high surface area carbon black. J. Electrochem. Chem. **535**(1-2), 113–119 (2002)
4. H. Meng, N. Larouche, M. Lefèvre, F. Jaouen, B. Stansfield, J. Dodelet, Iron porphyrin-based cathode catalysts for polymer electrolyte membrane fuel cells: Effect of NH3 and Ar mixtures as pyrolysis gases on catalytic activity and stability. Electrochim. Acta **55**(22), 6450–6461 (2010)
5. M.S. Shafeeyan, W. Mohd, A. Wan, A. Houshmand, A. Shamiri, A review on surface modification of activated carbon for carbon dioxide adsorption. J. Anal. Appl. Pyrolysis **89**(2), 143–151 (2010)
6. M.A. Montes-Morán, D. Suárez, J.A. Menéndeza, E. Fuente, On the nature of basic sites on carbon surfaces: an overview. Carbon N. Y. **42**(7), 1219–1225 (2004)
7. C. . Leon y Leon, J. . Solar, V. . Calemma, and L. . Radovic, Carbon N. Y. 30, 797 (1992), Evidence for the protonation of basal plane sites on carbon, 5, 811
8. K.B. Bota, M.K. Abotsi, C. Atlanta, Ammonia: a reactive medium for catalysed coal gasification. Fuel **73**(8), 1354–1357 (1994)
9. B. Stohr, H.P. Boehm, Enhancement of the catalytic activity of activated carbons in oxidation reactions by thermal treatment with

ammonia or hydrogen cyanide and observation of a superoxide species as a possible intermediate. Carbon N. Y. **29**(6), 707–720 (1991)
10. A.C. Garcia, E.A. Ticianelli, Investigation of the oxygen reduction reaction on Pt–WC/C electrocatalysts in alkaline media. Electrochim. Acta **106**, 453–459 (2013)
11. A.M. Gómez-Marín, J.L. Bott-Neto, J.B. Souza, T.L. Silva, W. Beck, L.C. Varanda, E.A. Ticianelli, Electrocatalytic Activity of Different Phases of Molybdenum Carbide/Carbon and Platinum-Molybdenum Carbide/Carbon Composites toward the Oxygen Reduction Reaction. ChemElectroChem **3**(10), 1570–1579 (2016)
12. J.L. Bott-Neto, W. Beck, L.C. Varanda, E.A. Ticianelli, Electrocatalytic activity of platinum nanoparticles supported on different phases of tungsten carbides for the oxygen reduction reaction. Int. J. Hydrog. Energy **42**(32), 20677–20688 (2017)
13. V.M. Nikolic, I.M. Perovic, N.M. Gavrilov, I.A. Pašti, A.B. Saponjic, P.J. Vulic, S.D. Karic, B.M. Babic, M.P. Marceta Kaninski, On the tungsten carbide synthesis for PEM fuel cell application – Problems, challenges and advantages. Int. J. Hydrog. Energy **39**(21), 11175–11185 (2014)
14. Y.C. Kimmel, X. Xu, W. Yu, X. Yang, J.G. Chen, Trends in Electrochemical Stability of Transition Metal Carbides and Their Potential Use As Supports for Low-Cost Electrocatalysts. ACS Catal. **4**(5), 1558–1562 (2014)
15. K. Huang, K. Bi, J.C. Xu, C. Liang, S. Lin, W.J. Wang, T.Z. Yang, Y.X. Du, R. Zhang, H.J. Yang, D.Y. Fan, Y.G. Wang, M. Lei, Novel graphite-carbon encased tungsten carbide nanocomposites by solid-state reaction and their ORR electrocatalytic performance in alkaline medium. Electrochim. Acta **174**, 172–177 (2015)
16. U.A. do Rêgo, T. Lopes, J.L. Bott-Neto, A.A. Tanaka, E.A. Ticianelli, Oxygen reduction electrocatalysis on transition metal-nitrogen modified tungsten carbide nanomaterials. J. Electroanal. Chem. **810**, 222–231 (2018)
17. S. Bukola, B. Merzougui, A. Akinpelu, M. Zeama, Cobalt and Nitrogen Co-Doped Tungsten Carbide Catalyst for Oxygen Reduction and Hydrogen Evolution Reactions. Electrochim. Acta **190**, 1113–1123 (2016)
18. J.G. Chen, Carbide and Nitride Overlayers on Early Transition Metal Surfaces: Preparation, Characterization, and Reactivities. Chem. Rev. **96**(4), 1477–1498 (1996)
19. M. Lefèvre, J.P. Dodelet, Fe-based catalysts for the reduction of oxygen in polymer electrolyte membrane fuel cell conditions: determination of the amount of peroxide released during electroreduction and its influence on the stability of the catalysts. Electrochim. Acta **48**(19), 2749–2760 (2003)
20. S.H. Liu, J.R. Wu, F.S. Zheng, J.M. Guo, Impact of iron precursors on the properties and activities of carbon-supported Fe-N oxygen reduction catalysts. J. Solid State Electrochem. **19**(5), 1381–1391 (2015)
21. C.W.B. Bezerra, L. Zhang, K. Lee, H. Liu, E.P. Marques, H. Wang, J. Zhang, A review of Fe–N/C and Co–N/C catalysts for the oxygen reduction reaction. Electrochim. Acta **53**(15), 4937–4951 (2008)
22. F. Jaouen, J.P. Dodelet, O2Reduction Mechanism on Non-Noble Metal Catalysts for PEM Fuel Cells. Part I: Experimental Rates of O2Electroreduction, H2O2Electroreduction, and H2O2Disproportionation. J. Phys. Chem. C **113**(34), 15422–15432 (2009)
23. J.S. Lee, S.T. Oyama, M. Boudart, Molybdenum carbide catalysts I. Synthesis of unsupported powders. J. Catal. **106**(1), 125–133 (1987)
24. P.F. Collins, H. Diehl et al., 2,4,6-Tripyridyl-s-triazine as a reagent iron determination of iron in limestone, silicates and refractories. Anal. Chem. **31**, 1862–1866 (1959)
25. L.G.R.A. Santos, C.H.F. Oliveira, I.R. Moraes, E.A. Ticianelli, Oxygen reduction reaction in acid medium on Pt–Ni/C prepared by a microemulsion method. J. Electroanal. Chem. **596**(2), 141–148 (2006)
26. I. Takahashi, S.S. Kocha, Examination of the activity and durability of PEMFC catalysts in liquid electrolytes. J. Power Sources **195**(19), 6312–6322 (2010)
27. T. Ungár, J. Gubicza, G. Ribárik, C. Pantea, T.W. Zerda, Microstructure of carbon blacks determined by X-ray diffraction profile analysis. Carbon N. Y. **40**(6), 929–937 (2002)
28. Z.Q. Li, C.J. Lu, Z.P. Xia, Y. Zhou, Z. Luo, X-ray diffraction patterns of graphite and turbostratic carbon. Carbon N. Y. **45**(8), 1686–1695 (2007)
29. T. Denaro, V. Baglio, M. Girolamo, V. Antonucci, A.S. Arico, F. Matteucci, R. Ornelas, Journ Appl. Electrochem **39**(11), 2173–2179 (2009)
30. B.L. Tang, Y. Wang, Y. Li, H. Feng, J. Lu, J. Li, Preparation, Structure, and Electrochemical Properties of Reduced Graphene Sheet Films. Adv. Funct. Mater. **19**(17), 2782–2789 (2009)
31. M.A.P. Almeida, L.S. Cavalcante, C. Morilla-Santos, C.J. Dalmaschio, S. Rajagopal, M.S. Li, E. Longo, Effect of partial preferential orientation and distortions in octahedral clusters on the photoluminescence properties of FeWO4 nanocrystals. CrystEngComm **14**(21), 7127 (2012)
32. K. Jiang, Q. Jia, M. Xu, D. Wu, L. Yang, G. Yang, L. Chen, G. Wang, X. Yang, A novel non-precious metal catalyst synthesized via pyrolysis of polyaniline-coated tungsten carbide particles for oxygen reduction reaction. J. Power Sources **219**, 249–252 (2012)
33. A.L. Patterson, The Scherrer Formula for X-Ray Particle Size Determination. Phys. Rev. **56**(10), 978–982 (1939)
34. S. Adhikari, D. Sarkar, H.S. Maiti, Synthesis and characterization of WO3 spherical nanoparticles and nanorods. Mater. Res. Bull. **49**, 325–330 (2014)
35. Y. Li, C. Guo, J. Li, W. Liao, Z. Li, J. Zhang, C. Chen, Pyrolysis-induced synthesis of iron and nitrogen-containing carbon nanolayers modified graphdiyne nanostructure as a promising core-shell electrocatalyst for oxygen reduction reaction. Carbon N. Y. **119**, 201–210 (2017)
36. L. Cao, Z. Lin, J. Huang, X. Yu, X. Wu, B. Zhang, Y. Zhan, F. Xie, W. Zhang, J. Chen, W. Xie, W. Mai, H. Meng, Nitrogen doped amorphous carbon as metal free electrocatalyst for oxygen reduction reaction. Int. J. Hydrog. Energy **42**(2), 876–885 (2017)
37. T. Jawhari, A. Roid, J. Casado, Raman spectroscopic characterization of some commercially available carbon black materials. Carbon N. Y. **33**(11), 1561–1565 (1995)
38. W. Zhang, Y. Xia, J. Ju, Y. Fan, Z. Fang, L. Wang, Z. Wang, Raman analysis of laser annealed nitrogen doped amorphous carbon film. Solid State Commun. **123**(3-4), 97–100 (2002)
39. D. Malko, T. Lopes, E. Symianakis, A.R. Kucernak, The intriguing poison tolerance of non-precious metal oxygen reduction reaction (ORR) catalysts. J. Mater. Chem. A Mater. Energy Sustain. **4**(1), 142–152 (2016)
40. W. Ding, Z. Wei, S. Chen, X. Qi, T. Yang, J. Hu, D. Wang, L.-J. Wan, S.F. Alvi, L. Li, Angew. Chem. Int. **52**(45), 11755–11759 (2013)
41. J.R. Perls, F. Kapteijn, J.A. Moulijn, Q. Zhu, M. Thomas, Evolution of nitrogen functionalities in carbonaceous materials during pyrolysis. Carbon N. Y. **33**(11), 1641–1653 (1995)
42. I. Kusunoki, M. Sakai, Y. Igari, S. Ishidzuka, T. Takami, XPS study of nitridation of diamond and graphite with a nitrogen ion beam. Surf. Sci. **492**(3), 315–328 (2001)
43. J. Liu, P. Song, W. Xu, Structure-activity relationship of doped-nitrogen (N)-based metal-free active sites on carbon for oxygen reduction reaction. Carbon N. Y. **115**, 763–772 (2017)
44. K. Wang, Y. Wang, Y. Tong, Z. Pan, S. Song, A Robust Versatile Hybrid Electrocatalyst for the Oxygen Reduction Reaction. ACS Appl. Mater. Interfaces **8**(43), 29356–29364 (2016)

45. U.I. Koslowski, I. Herrmann, P. Bogdanoff, C. Barkschat, S. Fiechter, N. Iwata, H. Takahashi, H. Nishikori, ECS Trans. **13**, 125 (2008)
46. K. Artyushkova, A. Serov, S. Rojas-Carbonell, P. Atanassov, Chemistry of Multitudinous Active Sites for Oxygen Reduction Reaction in Transition Metal–Nitrogen–Carbon Electrocatalysts. J. Phys. Chem. C **119**(46), 25917–25928 (2015)
47. T. Yamashita, P. Hayes, Analysis of XPS spectra of Fe2+ and Fe3+ ions in oxide materials. Appl. Surf. Sci. **254**(8), 2441–2449 (2008)
48. T. Mathew, N.R. Shiju, V.V. Bokade, B.S. Rao, C.S. Gopinath, Selective Catalytic Synthesis of 2-Ethyl Phenol over Cu1-xCoxFe2O4–Kinetics, Catalysis and XPS Aspects. Catal. Letters **94**(3/4), 223–236 (2004)
49. T. Mathew, S. Shylesh, B.M. Devassy, M. Vijayaraj, C.V.V. Satyanarayana, B.S. Rao, C.S. Gopinath, Selective production of orthoalkyl phenols on Cu0.5Co0.5Fe2O4: a study of catalysis and characterization. Appl. Catal. A **273**(1-2), 35–45 (2004)
50. B. Zhang, Z. Lin, J. Huang, L. Cao, X. Wu, X. Yu, Y. Zhan, F. Xie, W. Zhang, J. Chen, W. Mai, W. Xie, H. Meng, Highly active and stable non noble metal catalyst for oxygen reduction reaction. Int. J. Hydrog. Energy **42**(15), 10423–10434 (2017)
51. A. Velázquez-Palenzuela, L. Zhang, L. Wang, P.L. Cabot, E. Brillas, K. Tsay, J. Zhang, Carbon-Supported Fe–NxCatalysts Synthesized by Pyrolysis of the Fe(II)–2,3,5,6-Tetra(2-pyridyl)pyrazine Complex: Structure, Electrochemical Properties, and Oxygen Reduction Reaction Activity. J. Phys. Chem. C **115**(26), 12929–12940 (2011)
52. J. Zhang, J. Chen, Y. Jiang, F. Zhou, G. Wang, R. Wang, Tungsten carbide encapsulated in nitrogen-doped carbon with iron/cobalt carbides electrocatalyst for oxygen reduction reaction. Appl. Surf. Sci. **389**, 157–164 (2016)
53. G.-L. Li, C.-D. Liu, S.-M. Chen, C. Hao, G.-C. Cheng, Y.-Y. Xie, Promotion of oxygen reduction performance by Fe 3 O 4 nanoparticles support nitrogen-doped three dimensional meso/macroporous carbon based electrocatalyst. Int. J. Hydrog. Energy **42**(7), 4133–4145 (2017)
54. M.C. Weidman, D.V. Esposito, Y.-C.C. Hsu, J.G. Chen, Comparison of electrochemical stability of transition metal carbides (WC, W2C, Mo2C) over a wide pH range. J. Power Sources **202**, 11–17 (2012)
55. M.C. Weidman, D.V. Esposito, I.J. Hsu, J.G. Chenz, Electrochemical Stability of Tungsten and Tungsten Monocarbide (WC) Over Wide pH and Potential Ranges. J. Electrochem. Soc. **157**(12), F179 (2010)
56. D. Malko, A. Kucernak, T. Lopes, Performance of Fe–N/C Oxygen Reduction Electrocatalysts toward NO2–, NO, and NH2OH Electroreduction: From Fundamental Insights into the Active Center to a New Method for Environmental Nitrite Destruction. J. Am. Chem. Soc. **138**(49), 16056–16068 (2016)
57. T. Lopes, A. Kucernak, D. Malko, E.A. Ticianelli, Mechanistic Insights into the Oxygen Reduction Reaction on Metal-N-C Electrocatalysts under Fuel Cell Conditions. ChemElectroChem **3**(10), 1580–1590 (2016)
58. C.H. Choi, W.S. Choi, O. Kasian, A.K. Mechler, M.T. Sougrati, S. Brüller, K. Strickland, Q. Jia, S. Mukerjee, K.J.J. Mayrhofer, F. Jaouen, Unraveling the Nature of Sites Active toward Hydrogen Peroxide Reduction in Fe-N-C Catalysts. Angew. Chemie Int. Ed. **56**(30), 8809–8812 (2017)
59. H. Meng, W. Ouyang, F. Xie, W. Zhang, J. Chen, D. Yuan, J. Electrochem. Soc. **163**, 1373 (2016)
60. P.H. Matter, L. Zhang, U.S. Ozkan, The role of nanostructure in nitrogen-containing carbon catalysts for the oxygen reduction reaction. J. Catal. **239**(1), 83–96 (2006)
61. T. Lopes, P. Olivi, Non-precious Metal Oxygen Reduction Reaction Catalysts Synthesized Via Cyanuric Chloride and N-Ethylamine. Electrocatalysis **5**(4), 396–401 (2014)
62. A. Jing Liu, Carbon N. Y. **115**, 763 (2017)
63. D. Malko, A. Kucernak, Kinetic isotope effect in the oxygen reduction reaction (ORR) over Fe-N/C catalysts under acidic and alkaline conditions. Electrochem. Commun. **83**, 67–71 (2017)
64. D. Banham, S. Ye, Current Status and Future Development of Catalyst Materials and Catalyst Layers for Proton Exchange Membrane Fuel Cells: An Industrial Perspective. ACS Energy Lett. **2**(3), 629–638 (2017)